ELSEVIER

Chemical Engineering Science 62 (2007) 2663–2678

Chemical Engineering Science

www.elsevier.com/locate/ces

Catalytic hydrogenation of *o*-nitroanisole in a microreactor: Reactor performance and kinetic studies

Sunitha Tadepalli*, Raghunath Halder, Adeniyi Lawal

New Jersey Center for Micro chemical Systems, Department of Chemical, Biomedical and Materials Engineering, Stevens Institute of Technology, Hoboken, NJ 07030, USA

Received 23 May 2006; received in revised form 14 December 2006; accepted 22 December 2006
Available online 16 January 2007

Abstract

Hydrogenation of *o*-nitroanisole to *o*-anisidine was conducted in a packed-bed microreactor as a model hydrogenation reaction of importance to the pharmaceutical and fine chemicals industries with the aim of investigating the reactor performance and kinetics of the reaction. The effects of different processing conditions viz. hydrogen pressure, *o*-nitroanisole concentration, temperature, and residence time on the conversion of *o*-nitroanisole, space-time yield (STY), and selectivity of *o*-anisidine were studied using 2% Pd/zeolite catalyst. The kinetic study was undertaken in a differential reactor mode keeping the conversion of *o*-nitroanisole at less than 10%. During the kinetic study, it was observed that the intermediate 2-methoxynitrosobenzene was present in the reactor at low catalyst loading and low conversions because of short residence time in the reactor. Therefore, for the kinetics study, the overall reaction was treated as comprising two separate reactions: first the reduction of *o*-nitroanisole to 2-methoxynitrosobenzene and then, the reduction of 2-methoxynitrosobenzene to *o*-anisidine. Internal and external mass and heat transfer limitations in the microreactor were examined. Different rate laws using different mechanisms from the literature were considered to fit the experimental data. Two rate equations for the two consecutive reactions assuming Langmuir–Hinshelwood mechanism provided the best fit to the experimental data. These two rate equations predicted the experimental rates within 10% error. Experiments were also carried out in an integral reactor, and the reactor performance data were found to be in agreement with the predictions of the theoretical models.

Keywords: Catalytic hydrogenation; Fixed-bed microreactor; Reactor modeling; Kinetics

1. Introduction

Hydrogenation of *o*-nitroanisole to *o*-anisidine is one of the most common reactions in the fine chemicals and pharmaceutical industries. The commercial importance of *o*-anisidine has long been recognized. It is an intermediate in the manufacture of azo, napthol pigments and dyes which are used for paper manufacture, textile dying, agrochemicals and pharmaceuticals. Because of its wide applications, the production of *o*-anisidine is gaining importance; and hence has increased the need for the reduction of *o*-nitroanisole to *o*-anisidine.

Catalytic hydrogenation of *o*-nitroanisole using platinum group catalysts is the most common method of producing *o*-anisidine (Fig. 1). This method provides high selectivity and yields of *o*-anisidine at low cost. In the pharmaceutical industry, a significant number of the catalytic reactions are usually carried out in slurry semi-batch reactors, where the catalyst is suspended in the liquid which is continuously agitated with a stirrer. Other types of reactor designs commonly used for conducting catalytic reactions include trickle-bed, fluidized-bed and conventional packed-bed configurations. In these reactors, the reaction kinetics for fast gas–liquid–solid reactions is often limited by external mass transfer of gas to the catalyst surface. This is because of poor gas/liquid/solid contact provided by these reactors. As a result, the reaction volume is oversized in terms of the active volume leading to low yield of the product.

Hydrogenation of nitro compounds falls under the class of reactions which are fast on noble-metals and are usually limited by external mass transfer in conventional reactors (Figueras and Coq, 2001; Frikha et al., 2006). Besides, these reactions are highly exothermic in nature which necessitates effective

* Corresponding author. Tel.: +1 201 216 5332.
E-mail address: stadepal@stevens.edu (S. Tadepalli).

0009-2509/$ - see front matter © 2007 Elsevier Ltd. All rights reserved.
doi:10.1016/j.ces.2006.12.058

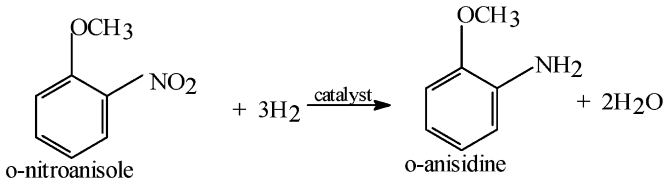

Fig. 1. Reaction scheme of hydrogenation of *o*-nitroanisole.

heat removal. In the pharmaceutical industry, the heat generated from these reactions usually requires several hundred tons of refrigeration controlled by a centralized system leading to huge energy requirements. Also, the non-uniform temperature distribution in the conventional reactors may develop hot spots on the catalyst surface or may lead to the formation of several byproduct(s) or intermediate(s) which can also react with one another, and further lead to violent decomposition of nitro compounds or partially hydrogenated intermediates (Stoessel, 1993; Blaser et al., 2001). Therefore, good temperature control within the reactor is essential to increase the selectivity of the desired compounds, and also to prevent thermal explosion conditions.

Improvements to the existing reactor systems led to the invention of miniaturized reactor configurations such as microreactors and mini-structured catalyst beds to solve the problems associated with heat and mass transfer in conventional systems. Microreactors are miniaturized reactor systems with reactor channel characteristic dimensions in the sub-millimeter range. These devices have been investigated for a number of model gas–surface catalytic reactions, liquid-phase, gas–liquid reactions as well as some selected commercial demonstrations like partial oxidation reaction in fuel cells and fine chemicals production.

The use of a continuous microreactor for highly exothermic reactions enables uniform temperature control throughout the reactor because of the high surface-to-volume ratio in these reactors. Because the temperature of most of the tubular reactors is controlled through walls of the reactor, as the diameter of the tubular reactor increases, the reactor becomes increasingly hindered by temperature gradients thereby reducing the reactor performance. This has been demonstrated by Besser and Ouyang (2005) and Besser et al. (2005), who conducted experimental and simulation studies on CO preferential oxidation reaction in a microchannel reactor with thin film wall catalyst and conventional packed-bed reactors of 2 and 4 mm diameters. They observed increase in CO conversion with decrease in the reactor diameter from 4 to 2 mm and further increase in CO conversion with the microchannel reactor. The extremely efficient heat removal capacity of the microreactor eliminates temperature gradients and prevents the on-set of other side reactions (such as r-WGS reaction for preferential oxidation) that may result due to temperature gradients inside the reactor.

For most multi-phase reactions, which are usually limited by mass transfer effects, the microreactor also offers improved overall reaction rate and reactor performance when compared with conventional macroreactors. The small channel size of the microreactor enables efficient gas/liquid mixing and sufficient gas/liquid/solid contact for the reaction to be controlled by intrinsic kinetics. A considerable number of studies have been conducted to understand the application of microreactors to gas/liquid catalytic reactions. Monolith structures with channels of about 1 mm diameter have been extensively used for conducting hydrogenation reactions of nitro-aromatic compounds (Machado et al., 1999; Andersson et al., 1986; Broekhuis et al., 2001; Kreutzer et al., 2005b) and other compounds (Irandoust et al., 1989; Nijhuis et al., 2003; Kreutzer et al., 2001; Liu et al., 2005). In these reactors, the catalyst is deposited on the walls of the reactor resulting in low pressure drop. Besides, the segmented flow in these reactors provides enhanced mass transfer characteristics leading to high reaction rates and thereby, high throughput. A few research groups in Germany have also conducted nitro group hydrogenation in various microstructured reactors using catalysts integrated in the reactor in different forms (Födisch et al., 2002; Hessel et al., 2003, 2004). A microstructured falling film reactor was developed by Institut für Mikrotechnik Mainz (IMM) for conducting the hydrogenation of nitrobenzene to aniline where the catalyst Pd was deposited on the walls of the reactor. This reactor offered excellent heat removal capabilities for this reaction and also for the direct fluorination of aromatics (Hessel et al., 2000). They also proved that the conventional equations for mass transfer may not always be applicable in micro scale, and must be verified prior to use. The mass transfer coefficient values of their system were estimated to be in the range of 3–8 s^{-1} (Hessel et al., 2004), with the interfacial surface area per reactor volume in the range 9000–15 000 m^2/m^3. This gas–liquid mass transfer rate represents more than a 100-fold increase compared with values reported for conventional multi-phase reactor systems. Therefore excellent heat and mass transfer was demonstrated in a microreactor for the hydrogenation of nitrobenzene. However, the maximum conversion was about 82% with selectivity to aniline of 80%. Due to the short residence time in the microreactor, it is possible that some of the intermediates would be present in the product stream. Higher residence time is required for aniline formation in a microreactor.

Födisch et al. (2002) also investigated the liquid-phase hydrogenation of *p*-nitro toluene using a stack of porous microstructured aluminum wafers, aluminum wire pieces and conventional fixed-bed particles in a microreactor module. They observed that the conversion in the wafers ranged from 39% to 84%, in comparison to 85% conversion with the fixed-bed microreactor. The reason for this could be that the fixed-bed microreactor offers higher residence time in the reactor than the other modes of catalyst incorporation in the microreactor module. Although, fixed-bed microreactor offers improvements in thermal management and mass transfer, there are obvious problems of pressure drop with channel dimensions in micron scale especially when operating at high flow rates to increase the production rate. This problem can be overcome by distributing the flow into multiple channels (numbering up) so that the pressure drop in each channel is kept low and the throughput remains the same. Losey et al. (2001) compared

the performance of the multi-channel packed microreactor with the traditional multi-phase packed-bed reactors in terms of pressure drop and mass transfer. They observed tremendous improvement in the mass transfer efficiencies of the packed-bed microreactor while maintaining the same pressure drop as the traditional packed-bed reactors.

In consideration of all the above, and its special importance to the pharmaceutical industry, the hydrogenation of *o*-nitroanisole to *o*-anisidine was chosen as a model reaction in the present study to evaluate the performance of the packed-bed microreactor by studying the effects of various operating conditions on the reactor performance. Also, this reactor was used to study the kinetics of this reaction so that optimum reaction conditions can be determined for the design of the multi-channel reactor. The advantages of conducting kinetic studies in microreactor is the small size of the microreactor channel ensures isothermal conditions to be maintained necessary for kinetic characterization of highly exothermic reactions that is not easy to obtain in classical calorimetric or batch systems. Also, the enhanced mass transfer rate in the microreactor enables the reactor to be operated in the true kinetic controlled region.

The present study provides a detailed study of the kinetics of the reaction in a packed-bed microreactor using 2% Pd/zeolite catalyst. The significance of inter-phase and intraparticle mass and heat transfer effects have been analyzed and, based on the experimental data obtained in the kinetic region, rate equations were derived. The theoretical predictions from these equations were compared with the experimental data obtained in the integral reactor.

2. Experimental

In this section a list of the chemicals used for the experiments, and the description of the experimental setup are provided. The details of the experimental procedure and analysis of the product are also described. The catalyst 2% (w/w) Pd supported on zeolite (aluminum sodium silicate) (proprietary catalyst) was sieved to obtain a particle size distribution of 45–75 and 75–150 μm. The dispersion of palladium on the support was measured using TEM (FEG-TEM, Model CM20, Philips, Eindhoven, Netherlands) and was calculated to be around 36%. The surface area of the catalyst was 170–220 m^2/g measured by BET (multi-point BET technique, using Quantochrome Instruments Autosorb-1). The raw materials *o*-nitroanisole and *o*-anisidine were purchased from Sigma Aldrich, and used without any purification. The solvent methanol (CH_3OH) was obtained from Pharmco Products Inc. The hydrogen was purchased from Praxair. The mobile phase used for the HPLC analysis comprised de-ionized water and Acetonitrile (HPLC grade); the latter was purchased from Pharmco Products Inc. Fig. 2 shows the experimental setup used for conducting the reaction. Two gas lines, one for hydrogen reactant (H_2) and the other for nitrogen (N_2) are shown in the system. The purpose of the nitrogen line was to flush the reactor system at the end of each experiment.

The compressed gas flowed through the mass flow controller and was then mixed with the liquid stream using a tee connection. The liquid reactant solution (*o*-nitroanisole in methanol) was pumped through the system using HPLC pump. The combined gas–liquid mixture then entered the reactor. The reactor was made of SS316L with an outer diameter of 1.5875 mm and inner diameter of 0.775 mm. The total length of the packed reactor varied from 6 to 8 cm of which the catalyst was packed within 1–6 cm of the reactor (depending upon the catalyst loading required for the experiment) and the remaining length of the reactor was filled with inert glass beads of the same size range as the catalyst particles. The glass beads were used to prevent any fine catalyst particles from clogging the filter placed at the entrance and exit of the reactor. As a result the pressure drop across the reactor under all experimental conditions was always less than 10% of the reactor pressure. The reactor was immersed horizontally into a constant temperature water bath so as to maintain isothermal conditions. The pressure values at the entrance and the exit were measured using pressure transducers (PI). From the reactor, the reaction mixture passed through a sampling loop where the product was collected for analysis. From the sampling loop, the reaction mixture passed through the back pressure regulator. The back pressure regulator was used to build up the desired pressure during an experimental run. From the back pressure regulator, the mixture passed to a product receiver where the liquid was collected in a glass vessel, and was vented to the atmosphere.

Before starting any experimental run, the reacting vapor effluent and product species from the previous run were purged from the system by replacing the reactor with an empty tube, and then nitrogen gas was passed, followed by the pure solvent. The packed reactor for the experimental run was then placed into the system. A reaction run was made by first pumping the liquid (*o*-nitroanisole in methanol) through the system at a flow rate of approximately 2.0–2.5 mL/min. A few minutes after the liquid emerged at the receiver, the back pressure regulator was partially closed until the desired pressure was attained. The liquid flow rate was then adjusted to the desired value, and the back pressure regulator adjusted to maintain the desired pressure in the system. The hydrogen gas was then passed through the system. The flow rate of hydrogen was controlled to the desired value using the mass flow controller. The reactor temperature was maintained at the desired value using the water bath. After the system attains steady state, the product was collected from the sampling loop by by-passing the stream. All experiments were conducted for a minimum period of 8 h during which the activity of the catalyst was close to its initial activity. The product samples were collected at regular intervals of 30 min. These samples were diluted with methanol (HPLC grade) and were analyzed using the high performance liquid chromatography (HPLC) manufactured by Shimadzu. A diode array detector was used for scanning so that the samples could be scanned at multiple wavelengths at the same time. A method was established in the HPLC using water and acetonitrile as the mobile phase, in conjunction with an RP C^{18} column from Waters Corporation. Calibration was done for both the reactant and the product using standard solutions. The concentrations of reactant and the product in the unknown product samples were determined using the calibration. The concentration of

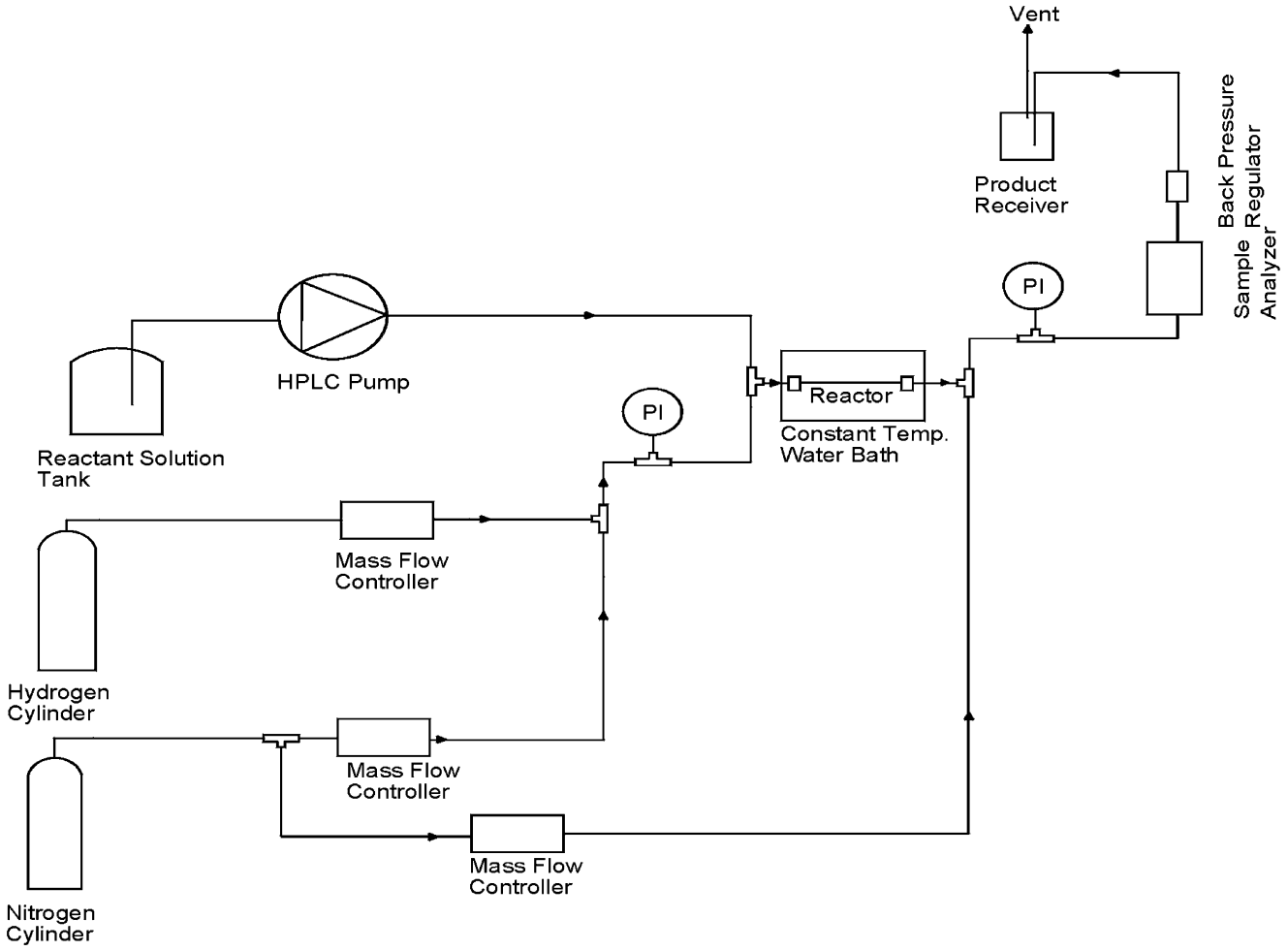

Fig. 2. Lab setup for hydrogenation of pharmaceutical intermediate.

the intermediate 2-methoxynitrosobenzene was calculated from material balance.

3. Results and discussion

In this section we will first provide a brief description of the reaction in general followed by a discussion of the study on fluid flow characterization and the effects of different operating conditions using 2% Pd/zeolite catalyst to determine the best operating regime for maximum yield of *o*-anisidine in a microreactor (Sections 3.1 and 3.2). Then, we present the kinetics study of the reaction in Section 3.3.

The catalytic hydrogenation of *o*-nitroanisole to *o*-anisidine involves a three-step reduction series reaction. First, the reduction of *o*-nitroanisole to 2-methoxynitrosobenzene, next to *N*-(2-methoxyphenyl) hydroxylamine, and, finally to *o*-anisidine. During the experiments only one intermediate was observed in the product stream along with the product, and reactant at all operating conditions. This intermediate was found to be 2-methoxynitrosobenzene by the mass spectrum analysis. The presence of hydroxylamine derivative was not detected during analysis, indicating that it had only transient lifetime probably because of its instantaneous reaction with hydrogen to form *o*-anisidine, the rate of which far exceeds its formation from 2-methoxynitrosobenzene. Thus the hydrogenation of *o*-nitroanisole to *o*-anisidine was considered as a process consisting of two consecutive reactions, one leading to the formation of 2-methoxynitrosobenzene, and the other leading to the formation of *o*-anisidine.

3.1. Fluid flow characterization

The fluid dynamics of reactors involving multi-phase flow has significant effect on the reactor performance. It is critical to understand the hydrodynamics in the microreactor before attempting to study the effect of operating conditions and the kinetics of the reaction in the microreactor. Various flow regimes ranging from bubbly flow to annular flow exists in small channel diameters (between 0.5 and 5 mm) at different gas and liquid flow velocities (Kreutzer et al., 2001, 2005a). We conducted flow visualization experiments using a transparent glass tube with the same dimensions as the microreactor. The liquid flow rates used in these experiments varied from 0.03 to 0.2 mL/min and gas flow rates from 2 to 10 sccm. During these experiments,

a two-phase flow pattern known as *Taylor flow*, with alternating gas and liquid slugs was observed in the empty microreactor under all operating conditions. Numerical simulation using CFD and Fluent also proved that Taylor flow exists under these flow conditions (Qian and Lawal, 2006).

Similar flow visualization experiments were conducted in a glass microreactor with a square cross section measuring 500 μm × 500 μm packed with glass beads of the same size range as the catalyst particles used in all experiments. These experiments showed that Taylor flow regime exists in a packed-bed microreactor as well, except that slug boundaries are broken-up by the particles. This type of flow is known as transitional Taylor flow. During gas–liquid reactions in micro channels, Taylor flow has been shown to enhance mass transfer significantly (Kreutzer et al., 2001). Therefore, for all the experiments reported here, the reactor was operated in Taylor flow regime.

3.2. Effect of operating conditions on reactor performance

The effect of operating conditions on the reactor performance was studied by comparing the conversion of *o*-nitroanisole, *selectivity* and *space–time yield* (*STY*) of *o*-anisidine under different reaction conditions. *Selectivity* is defined as the ratio of the number of moles of the desired product formed to the moles of the product that would have been formed if there were no side reactions. STY is the rate of formation of the desired product per unit mass of the active metal (Pd) in the catalyst.

3.2.1. Effect of pressure on conversion, selectivity and STY

To study the effect of pressure on conversion of *o*-nitroanisole, selectivity and STY of *o*-anisidine, experiments were carried out in the pressure range of 50–250 psig at a substrate concentration of 1.299 mol/L in methanol, temperature of 30 °C and constant residence time. The residence time was kept constant by varying the catalyst loading. Fig. 3 shows a plot of the conversion vs. pressure at a constant residence time of 1.1 s (inlet conditions). Fig. 3 indicates that the conversion remains almost constant with increase in pressure, but the STY increases with increase in pressure in the range of pressures studied. This increase in STY is attributed to the increase in the concentration of dissolved hydrogen with increase in pressure, thereby resulting in a higher reaction rate. However, pressure has no effect on the conversion at constant residence time because the increase in the reaction rate at higher pressure is countered by the decrease in the catalyst loading.

3.2.2. Effect of temperature on conversion, selectivity and STY

To study the effect of temperature on conversion of *o*-nitroanisole, selectivity and STY of *o*-anisidine, experiments were carried out in the temperature range of 25–55 °C at a substrate concentration of 1.299 mol/L in methanol, pressure of 50 psig and a catalyst (2% Pd/zeolite) loading of 6.9 mg. The liquid and hydrogen gas flow rates were 0.05 mL/min and 5 sccm, respectively. Fig. 4 shows that with increase in temperature, both the conversion and STY increase while the selectivity remains close to 100% at all the temperature levels. The trend in STY indicates that the reaction may be controlled by intrinsic kinetics, because the average reaction rate almost doubles for every 10° increase in temperature. If the reaction were controlled by mass transfer there will be very slight increase in reaction rate with increase in temperature. However, this conclusion cannot be confirmed until the absence of mass transfer resistances both external and internal, has been established. The role played by mass transfer resistances in the kinetics of the reaction will be discussed in the kinetics section.

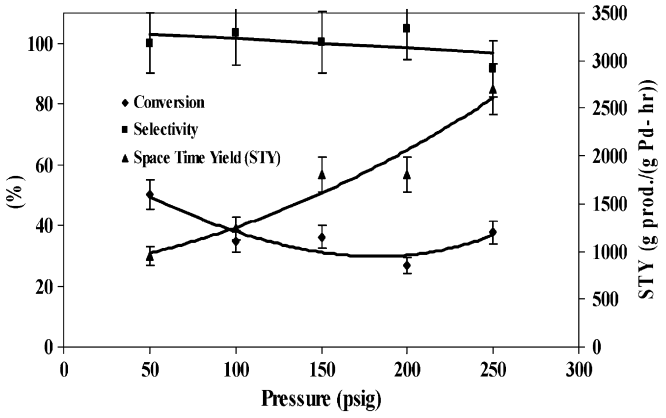

Fig. 3. Effect of pressure on reactor performance based on a constant residence time (1.1 s). (All the runs were made at 30 °C, liquid (1.299 mol/L *o*-nitroanisole in methanol) flow rate = 0.05 mL/ min, H_2 flow rate = 5 sccm, 2% Pd/zeolite catalyst.)

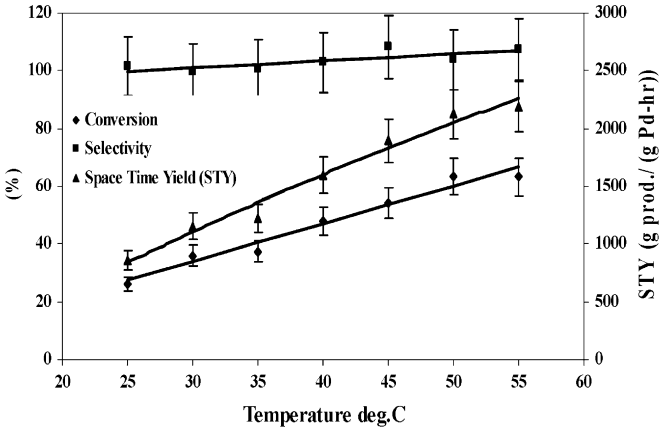

Fig. 4. Effect of temperature on reactor performance. (All the runs were made at a pressure of 50 psig, liquid composition of 1.299 mol/L *o*-nitroanisole in methanol, liquid flow rate of 0.05 mL/min, H_2 flow rate of 5 sccm and with 6.9 mg of 2% Pd/zeolite catalyst.)

3.2.3. Effect of residence time on conversion, selectivity and STY

In the current experimental reactor system, since the microreactor is in the form of a packed-bed, it is important to define the residence time for this multi-phase reaction before we actually study the effect of varied residence time. Residence time can be defined as the total volume of the catalyst divided by the total superficial volumetric flow rate of the liquid and gas.

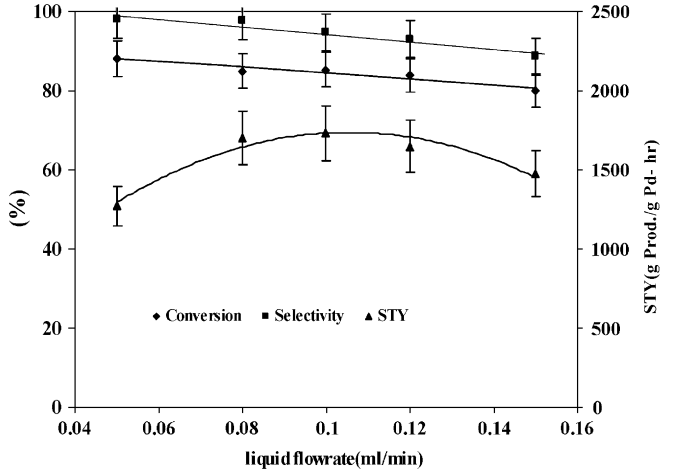

Fig. 5. Effect of liquid flow rate on reactor performance. (All runs were made at 45 °C, 100 psig reactor pressure, H_2 flow rate of 5 sccm, liquid feed containing 1.2 mol/L nitroanisole in methanol and 13 mg of 2% Pd/zeolite catalyst.)

Experiments for varying the residence time were done both by changing the liquid and gas flow rates, and also by changing the amount of catalyst in the reactor.

Experiments for varying the liquid flow rate were conducted to study its effect on the conversion of *o*-nitroanisole, selectivity and STY of *o*-anisidine. All the experiments were carried out at a temperature of 45 °C, substrate concentration of 1.2 mol/L in methanol, pressure of 100 psig and a catalyst (2% Pd/zeolite) loading of 13 mg. The flow rate of the liquid was varied in the range of 0.05–0.15 mL/min, and the H_2 flow rate was kept constant at 5 sccm. In these experiments, the actual gas flow rate is approximately 10 times the liquid flow rate. Therefore, a change in liquid flow rate does not change the residence time significantly. Fig. 5 shows the effect of liquid flow rate on the conversion, selectivity and STY. The data shows that the conversion decreases with increase in liquid flow rate while the selectivity remains almost constant. However, STY or the overall reaction rate first increases with increase in liquid flow rate up to a liquid flow rate of 0.1 mL/min, and then decreases with further increase in liquid flow rate.

In the experiments that we conducted to see the effect of the liquid flow rate at constant gas flow rate, it was observed that the liquid slug length increases with increase in the liquid flow rate. As the liquid slug length increases, the rate of convective mass transfer from gas to liquid decreases (Kreutzer et al., 2001). Small liquid slugs enhance the mass transfer from gas to the liquid. Therefore, conversion and STY increase with decrease in liquid flow rate (or decrease in liquid slug length). However, a decrease in STY below the liquid flow rate of 0.1 mL/min may be attributed to the high conversion of *o*-nitroanisole under these conditions that results in decrease of average reaction rate or STY.

Another method of changing the residence time is to change the gas flow rate. Experiments for varying the gas flow rate were conducted to study its effect on the conversion of *o*-nitroanisole, selectivity and STY of *o*-anisidine. All the experiments were carried out at a temperature of 45 °C, substrate concentration of 1.2 mol/L in methanol, pressure of 100 psig, liquid flow rate of 0.05 mL/min, and a catalyst (2% Pd/zeolite) loading of 13 mg. The effect of gas flow rate on conversion, STY and selectivity is shown in Fig. 6. With increase in gas flow rate, the conversion decreases while the selectivity remains at almost a constant value of 100%. In the range of gas flow rates considered, the STY remains almost constant with a negligible change. With increase in gas flow rates, the residence time of the reactants in the reactor decreases thereby decreasing the conversion. Therefore, higher residence time is needed for high conversion of *o*-nitroanisole. However, the STY remains the same even at high conversions because the increase in the conversion or yield at higher residence time is balanced by the increase in residence time.

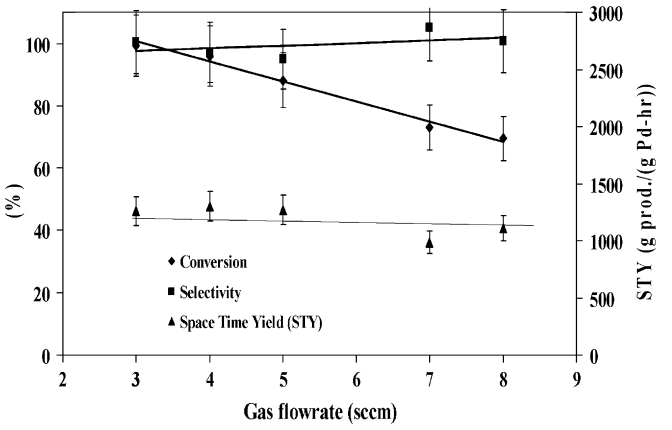

Fig. 6. Effect of gas flow rate on reactor performance. (All the runs were made at 45 °C, 100 psig reactor pressure, with 1.2 mol/L *o*-nitroanisole in methanol flow rate of 0.05 mL/min and 13 mg of 2% Pd supported on zeolite catalyst.)

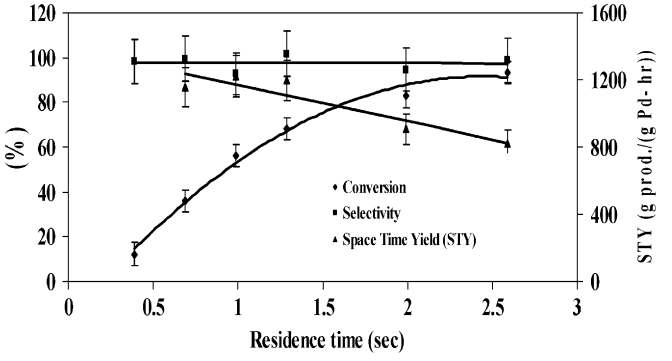

Fig. 7. Effect of residence time on reactor performance (based on catalyst loading). (All the runs were made at 30 °C, 50 psig pressure, 1.299 mol/L *o*-nitroanisole in methanol, liquid flow rate of 0.05 mL/min, H_2 flow rate of 5.0 sccm and 2% Pd/zeolite catalyst.)

The effect of residence time on the conversion, selectivity and STY was also studied by varying the catalyst loading, and keeping all the other operating conditions constant. All the experiments were carried out at a temperature of 30 °C, substrate concentration of 1.299 mol/L in methanol, pressure of 50 psig, liquid flow rate of 0.05 mL/min, and H_2 flow rate of 5 sccm. Fig. 7 shows the results obtained. Selectivity is close to 100%

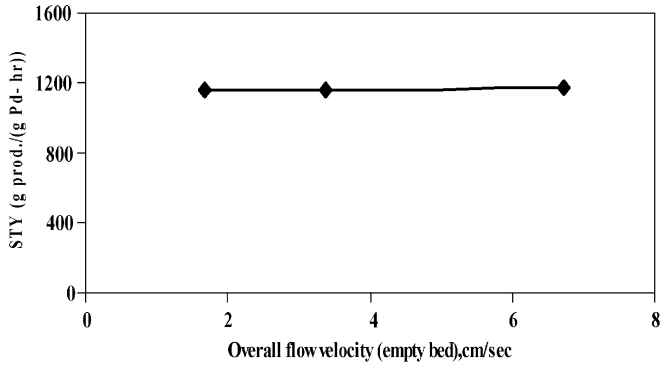

Fig. 8. Effect of overall flow velocity on overall reaction rate for the same residence time. (All runs were made at 30 °C, reactor pressure of 10 psig and 1.299 mol/L *o*-nitroanisole in methanol.)

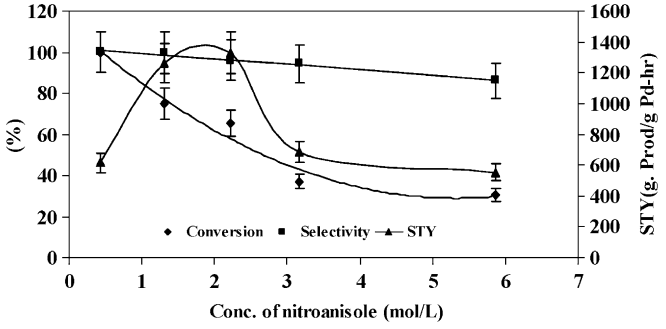

Fig. 9. Effect of nitroanisole concentration on reactor performance. (All runs were made at 45 °C, 50 psig reactor pressure, with a liquid flow rate of 0.05 mL/min, and gas flow rate of 5 sccm, and 13 mg of 2% Pd/zeolite catalyst.)

in all the runs. As expected the conversion increases with increase in catalyst loading. The value of STY decreases with increase in catalyst amount because the average reactant concentration decreases. Any of the three methods presented here can be used to change the residence time. However, when the residence time is varied by changing the flow velocity, then an additional variable may be introduced, namely the dependence of gas–liquid mass transfer coefficient on velocity. The effect of velocity was seen by measuring STY at the same residence time, but with different flow velocities. The residence time was kept constant by increasing the amount of catalyst in proportion to the increase in flow velocity. Fig. 8 shows the results obtained from these experiments. The data clearly show that the reaction rate is independent of the flow velocity. Therefore, within the range of conditions considered in this study, the residence time can be varied either by changing the catalyst loading or the liquid and gas flow rates.

3.2.4. *Effect of substrate concentration*

To study the effect of substrate concentration on reactor performance, experiments were carried out in the concentration range of 0.4–6 mol/L *o*-nitroanisole in methanol, temperature of 45 °C, 50 psig reactor pressure, and a catalyst loading of 13 mg of 2% Pd/zeolite. The liquid and hydrogen gas flow rates were 0.05 mL/min and 5 sccm respectively. Fig. 9 shows that decrease in *o*-nitroanisole concentration increases the conversion. The selectivity is lower at higher *o*-nitroanisole concentration indicating that the rate of intermediate formation may have a stronger dependency on the *o*-nitroanisole concentration. The STY increases up to nitroanisole concentration of 2.21 mol/L, and then starts to decrease thereafter. Mahajani and Haldar (2004) observed similar trend at high concentrations of *o*-nitroanisole while conducting experiments in a batch reactor. They observed that the rate of *o*-anisidine formation at high concentrations of *o*-nitroanisole is low because of substrate inhibition effect present at such high concentrations. Another reason could be that at such high concentrations, external mass transfer resistance may become significant because of the low solubility of hydrogen at high concentrations of the reactant (Brahme et al., 1982). Therefore low concentrations (0.4–2 mol/L) of *o*-nitroanisole were used for the kinetics studies.

3.3. *Kinetic studies*

Any three-phase catalytic reaction involves a series of mass transfer and reaction steps that contribute to the overall observed reaction rate. The step that has the greatest influence on the overall reaction rate is considered as the rate controlling or limiting step. From the bulk gas to the catalyst surface, the overall mass transfer resistance is determined by external mass transfer resistance and internal mass transfer resistance. External mass transfer resistance includes resistance to gas absorption at the gas–liquid interface and resistance to transport of the reactants to the catalyst surface. Internal mass transfer resistance refers to the resistance to diffusion of the reactants in the pores of the catalyst. The reaction is said to be controlled by external mass transfer if the external mass transfer resistance has a greater influence than the internal mass transfer resistance and the intrinsic reaction on the overall reaction rate. Similarly, the reaction is said to be controlled by internal mass transfer if the internal mass transfer resistance has a greater influence than the external mass transfer resistance and the intrinsic reaction on the overall reaction rate. The reaction is said to be kinetically controlled if both the external and internal mass transfer resistances are negligible.

Optimization of any process requires that the contributing rate steps are understood individually and that their impact on the total process rate is quantifiable. The influence of external mass transfer is especially significant in the case of multi-phase or three-phase reaction systems, which are often mass-transfer limited when operated under industrial conditions. In transitional Taylor flow observed in the packed microreactor, mass transfer of hydrogen to the catalyst surface can take place either directly in the gas slug or indirectly in the liquid slug region. The schematic representation of these mass transfer steps is depicted in Fig. 10. *Direct* mass transfer refers to transfer of hydrogen from the gas slug through the thin liquid film

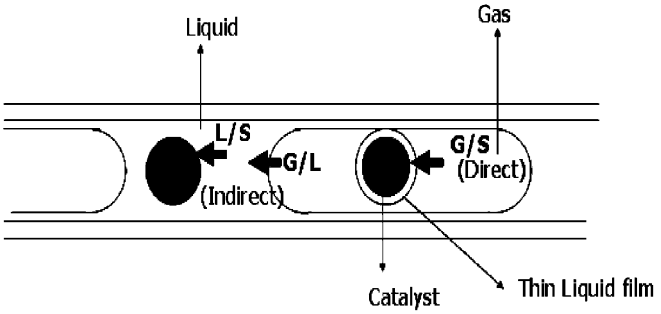

Fig. 10. Schematic representation of mass transfer steps in a packed-bed microreactor.

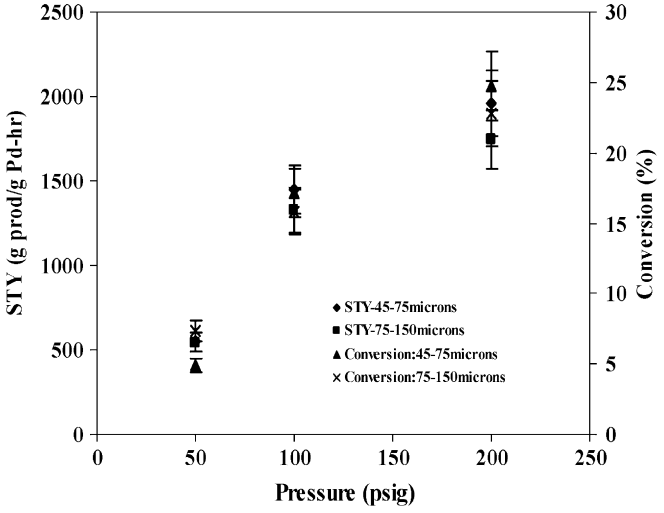

Fig. 11. Effect of particle size on STY and conversion at different pressures. (All runs were made with 1.299 mol/L *o*-nitroanisole in methanol, liquid flow rate of 0.05 mL/min, H_2 flow rate = 5 sccm, 2.2 mg of 2% Pd/zeolite catalyst and at 30 °C.)

surrounding the catalyst surface while *Indirect* mass transfer refers to transfer of hydrogen across the gas/liquid interface, then through the liquid slugs to the catalyst surface. Both direct and indirect mass transfers contribute equally to the overall external mass transfer.

To evaluate the possible mass transfer limitations, an experimental approach and a theoretical calculation procedure will be presented.

3.3.1. Analysis of internal mass transfer effect

The size of the catalyst particles is one of the most important factors influencing internal mass transfer resistance in catalytic reactions. Experiments were conducted using two different catalyst particle size ranges, 45–75 μm (average size = 60 μm) and 75–150 μm (average size = 112 μm) at different hydrogen pressure and reactor temperature levels to determine the effect of catalyst particle size on the STY, and the conversion of the reactant. The effect of particle size on STY and conversion at different pressure and temperature levels are shown in Figs. 11 and 12, respectively. The data in these figures indicate that both reactor performance parameters at all the temperature and pressure levels considered are nearly the same for the two particle sizes utilized. Hence, it can be concluded that the influence of internal diffusion on the reaction rate can be neglected for the range of pressures and temperatures studied. To further validate this conclusion, calculation of the catalyst effectiveness factor η_{eff} was performed. First order approximations were used for calculating effectiveness factor for the reactant most limiting (i.e., for which the diffusivity multiplied by the driving force was smallest). The effectiveness factor calculated under the reaction conditions ranges from 0.7 to 0.97. Since the effectiveness factor for these operating conditions is close to 1 ($\eta \rightarrow 1$), the calculations confirm the experimental data indicating that the hydrogen diffusion inside the catalyst pores does not affect the reaction rate significantly.

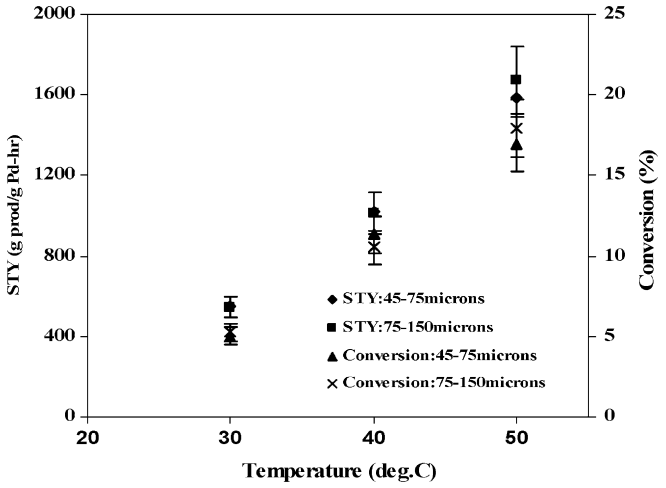

Fig. 12. Effect of particle size on STY and conversion at different temperature levels. (All runs were made with 1.299 mol/L *o*-nitroanisole in methanol, liquid flow rate of 0.05 mL/min, H_2 flow rate=5 sccm, 2.2 mg of 2% Pd/zeolite catalyst, at 50 psig pressure.)

3.3.2. Analysis of external mass transfer effect

A good test for the presence of external mass transfer effects is to see if the reaction rate increases with increase in fluid velocity. However, increasing the velocity in a packed-bed reactor may be inconclusive in most cases because an increase in the flow velocity for the same length of the catalytic bed will, in addition to its effect on mass transfer, increase the intrinsic rate of the reaction by increasing the average concentration (due to lower conversion at high velocities). This can be avoided by using catalyst beds of two different lengths and flow velocities, but same contact time (Satterfield, 1970). At the same contact time, the linear velocity will be greater in the longer bed; and in the absence of mass transfer limitations, the concentration profile and the degree of conversion will be the same for the two cases. Therefore, experiments were conducted following the outlined approach to see the effect of overall flow velocity on the STY and determine the controlling regime in this gas–liquid–solid reaction.

Fig. 13 shows the results obtained from these experiments which were conducted at a constant residence time by

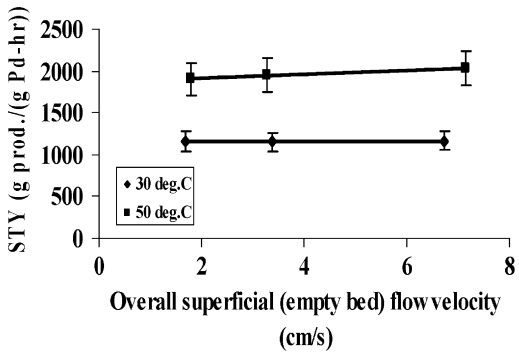

Fig. 13. Effect of overall flow velocity on reaction rate for the same residence time. (All runs were made at reactor pressure of 100 psig and 1.299 mol/L *o*-nitroanisole in methanol.)

varying the gas and liquid flow rates proportionately with the catalyst amounts so as to obtain constant residence time. The data clearly show that the reaction rate is independent of the flow velocity, which indicates the absence of external mass transfer limitations for the reaction under the present operating conditions.

To further validate this conclusion, quantitative criteria suggested by Mills and Chaudhari (1997) were used. Thus, the factors, α_1 and α_2 which represent the ratios of the observed rate of reaction to the maximum possible rates of gas–liquid and liquid–solid mass transfer rates, respectively, were calculated from the rate data. The gas to liquid mass transfer can be considered unimportant if

$$\alpha_1 = \frac{R_{\text{obs}}}{k_{gl}a_{gl}C_{\text{H}_2,\text{sat}}} < 0.1. \quad (1)$$

The saturated concentration of hydrogen in the reaction medium was obtained from the solubility data for H_2 in a mixture of *o*-nitroanisole-methanol from the work of Brahme et al. (1982). The values of $k_{gl}a_{gl}$ were obtained from the correlations available in the literature. The only available literature providing the values of mass transfer coefficients for packed-bed microreactor was that of Losey et al. (2001). They observed that the mass transfer coefficients values of their system were in the range of 5–15 s^{-1}. However, there are no correlations available in the literature for estimating the gas–liquid mass transfer coefficients in a packed-bed microreactor. Therefore, the correlations from trickle-bed (Versteeg et al., 1992; Iliuta et al., 1999) and monolith reactors (Kreutzer et al., 2001) were assumed to be the closest approximate for the mass transfer coefficient values in the packed-bed microreactor. The calculated values of α_1 using the correlations are much higher than 1 which is highly impossible. This suggests that the actual mass transfer coefficient in the packed-bed microreactor is much higher than the estimates obtained from these correlations. Since there are no reliable correlations for estimating the gas–liquid mass transfer coefficients for packed microreactor, experimental verification was considered as the only means of concluding that the reaction is not mass-transfer limited at the gas–liquid interface.

The liquid to solid mass transfer can be considered unimportant if

$$\alpha_2 = \frac{R_{\text{obs}}}{k_{ls}a_{ls}C_{\text{H}_2,\text{sat}}} < 0.1. \quad (2)$$

Two different correlations were used to estimate the values of $k_{ls}a_{ls}$. These correlations were based on monolith (Winterbottom et al., 2004) and trickle-bed reactors (Satterfield, 1970), respectively. The calculated values of α_2 from above correlations were less than 0.1. Therefore, one can convincingly conclude that liquid film diffusion does not limit the reaction rate. The calculations and the experimental data confirm that the reaction is not mass-transfer limited under the operating conditions utilized in the experiments.

3.3.3. Analysis of heat transfer effects

Apart from mass transfer limitations, heat transfer limitations can also have significant effect on the kinetics of the reaction. The intrusion of heat transfer resistances inside the reactor can lead to severe degradation in the catalyst's performance thus completely masking the true kinetics of the reaction. Efficient heat removal from the reactor is essential especially for hydrogenation reactions which are highly exothermic in nature. Microreactors generally offer excellent heat transfer rates because of high surface-to-volume ratio and short conduction paths. To ensure that the kinetic data obtained in an experimental reactor reflect only kinetic effects, the temperature gradients must be minimized from three domains: intraparticle-within the individual catalyst particles, interphase-between the external surface of the particles and fluid adjacent to them, and interparticle-between the local fluid regions or catalyst particles. Certain criteria are available in the literature (Mears, 1971a, b) to estimate whether heat transport effects in any domain are significantly affecting the experimental results. Mears (1971a) suggested that the heat transfer resistances are generally in the order of interparticle > interphase > intraparticle when the Biot number (Bi) is much smaller than 10. The Biot number expresses the ratio of thermal resistance of the particle to that of the film around the particle.

$$Bi = \frac{hd_p}{\lambda}. \quad (3)$$

In this calculation, d_p is the diameter of the catalyst particle $\sim 100\,\mu$m; the heat transfer coefficient (h) for the reactants is within the range of 10–100 W/m^2 K (Mears, 1971a) and the effective thermal conductivity (λ) is in the order of 0.1 W/m K for the porous catalyst (Ajmera et al., 2002). The calculated Biot number (0.0375) is much smaller than 10 which implies that the effect of interparticle heat transfer resistance is predominant over interphase or intraparticle heat transport resistance. Interparticle heat transport occurs both radially and axially within the reactor. Axial heat transport resistance can be neglected if the ratio of axial length of the reactor to the catalyst particle size is greater than 20. In the present study, since the microreactor length at typical reaction conditions is much greater than the catalyst particle size (> 30 times), axial heat transport resistance can be neglected. However, radial heat transfer effect

cannot be assumed to be negligible because radial temperature gradients can lead to reaction rates several thousand folds greater at the axis of the reactor than at the wall. A criterion for quantitative analysis of radial heat transport limitations is given by the Damkőhler number for heat transfer (Mears, 1971a) (*Da*) which is defined by the following equation:

$$Da = \left| \frac{-\Delta H(-r_{\text{obs}})(1-\varepsilon)R_0^2}{\lambda T_w(1+b)} \right| < 0.4\frac{RT_w}{E_a}. \quad (4)$$

If the left-hand side of the above equation is smaller than the right-hand side, the radial temperature difference in the reactor would be less than 5%. In the calculations, (ΔH) the heat of the reaction is 536 kJ/mol; the observed reaction rate (r_{obs}) from the experiments was obtained to be 42.12 mol/m^3 s at a temperature (T_w) of 30 °C, the radius of the tubular reactor (R_0) is 0.0003875 m, ε is the bed porosity which is assumed to be 0.3 and, b is the ratio of diluent to catalyst volume which is 49. The approximate activation energy for the reaction was obtained from the literature as 43.83 kJ/mol (Chaudhari et al., 1983). The calculations show that the left-hand side ($2.9 * 10^3$) is one order of magnitude smaller than the right-hand side ($3.1 * 10^4$). Hence, it can be concluded that the radial heat transfer effects can be neglected in the micro reactor. With all the above considerations, overall it can be concluded that under the present operating/processing conditions the reaction is controlled by surface kinetics and not significantly influenced by mass and heat transfer resistances.

3.3.4. Rate analysis using differential method

Although limited information is available in the literature on the kinetics of hydrogenation of *o*-nitroanisole (Chaudhari et al., 1983), it is reasonable to assume that *o*-nitroanisole behaves in a similar way to other aromatic nitro compounds (Yao and Emmett, 1961; Andersson et al., 1986; Neri et al., 1995) behave in a similar way as *o*-nitroanisole. Some researchers used Langmuir–Hinshelwood (L–H) and Eley–Rideal type models to describe the kinetics of the reaction (Chaudhari et al., 1983; Andersson et al., 1986). A mechanism for the hydrogenation of nitro compound was suggested by Winterbottom (1981) who described the detailed surface chemical kinetics of the reaction by splitting the overall reaction into six individual reactions. Based on this mechanism, different rate expressions were derived by assuming individual reactions as the rate limiting steps. Similarly Chaudhari et al. (1983) also investigated the kinetics of hydrogenation of *o*-nitroanisole on Pd/C catalyst. They used a rate equation for fitting their experimental kinetic data which was consistent with a mechanism in which desorption of the products is the rate controlling step.

Most of these kinetic studies are based on global kinetic rate models based on hydrogen consumption and overall conversion. This does not fully explain the role of individual intermediate species involved in the reaction. As was discussed earlier, in this study the overall reaction was considered to comprise two consecutive reactions, one leading to the formation of 2-methoxynitrosobenzene, and the other leading to the formation of *o*-anisidine. Experiments were conducted in the microreactor under different process conditions to determine the rate expressions for both reactions. The conversion in the microreactor was limited to 10% so that a differential reactor can be assumed to find the dependence of the reaction rates on the reactant concentrations.

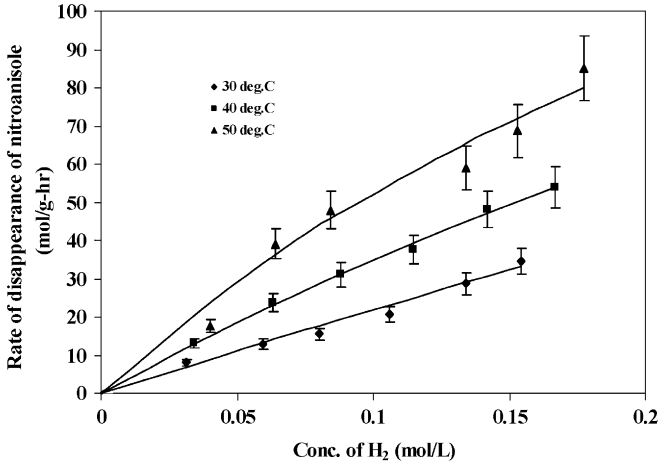

Fig. 14. Effect of H_2 concentration on the reaction rate of disappearance of *o*-nitroanisole.

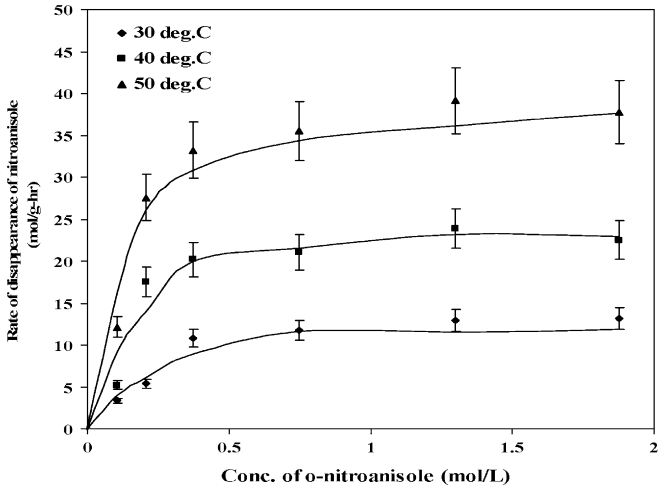

Fig. 15. Effect of *o*-nitroanisole concentration on the rate of disappearance of *o*-nitroanisole.

The effect of hydrogen concentration on the rate of disappearance of *o*-nitroanisole was investigated in a range of 50–300 psig, at temperatures of 30, 40 and 50 °C and *o*-nitroanisole concentration of 1.299 mol/L in methanol. The results are presented in Fig. 14. The rate of disappearance of *o*-nitroanisole increases almost linearly with increase in hydrogen concentration at constant *o*-nitroanisole concentration. The effect of *o*-nitroanisole concentration on the rate of disappearance of *o*-nitroanisole was investigated in the concentration range of 0.1–2 mol/L at temperatures of 30, 40 and 50 °C, and a hydrogen pressure of 100 psig. The results are presented in Fig. 15. The rate of disappearance of *o*-nitroanisole increases somewhat linearly with increase in *o*-nitroanisole

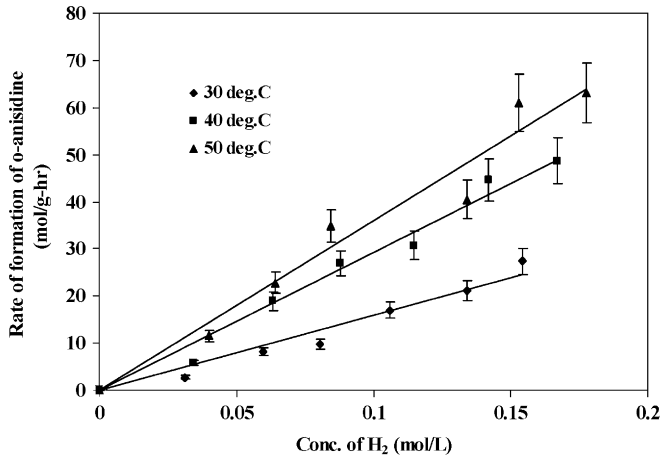

Fig. 16. Effect of H_2 concentration on the reaction rate of formation of *o*-anisidine.

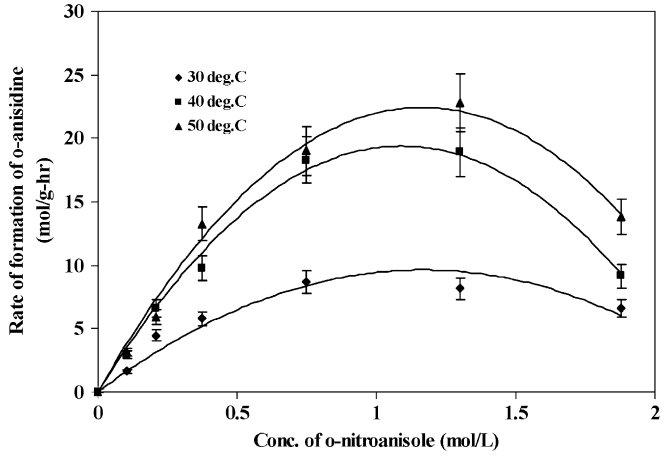

Fig. 17. Effect of *o*-nitroanisole concentration on the rate of formation of *o*-anisidine.

concentration up to a certain concentration and then remains constant, for all temperatures. This suggests that L–H expression should be considered for the rate equation. The effect of hydrogen concentration on the rate of formation of *o*-anisidine was investigated in a range of 50–300 psig at temperatures of 30, 40 and 50 °C, and *o*-nitroanisole concentration of 1.299 mol/L in methanol. The results are presented in Fig. 16. The average rate of *o*-anisidine formation increases linearly with increase in hydrogen concentration at constant *o*-nitroanisole concentration. The effect of *o*-nitroanisole concentration on the rate of formation of *o*-anisidine was investigated in a range of 0.1–2 mol/L *o*-nitroanisole in methanol), at temperatures of 30, 40 and 50 °C, and a hydrogen pressure of 100 psig. The results are presented in Fig. 17. The rate first increases with *o*-nitroanisole concentration, attains a maximum value and then decreases with further increase in *o*-nitroanisole concentration. Comparison of Figs. 15 and 17 indicates that the rate of *o*-nitroanisole disappearance is higher than the rate of formation of *o*-anisidine at the same conditions. The difference between the rate of disappearance of *o*-nitroanisole,

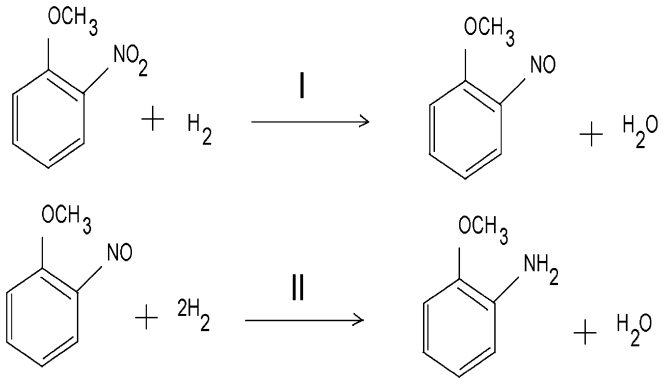

Fig. 18. Reaction pathway for the hydrogenation of *o*-nitroanisole.

and the rate of formation of *o*-anisidine at same *o*-nitroanisole concentration in the differential reactor is an indication of the presence of an intermediate(s). The intermediate 2-methoxy-nitrosobenzene is present in the product stream at low conversions of *o*-nitroanisole. Therefore the overall kinetics of *o*-nitroanisole hydrogenation to *o*-anisidine is split into two rate equationsderived for the two consecutive reactions shown in Fig. 18.

3.3.5. Kinetic modeling

The rate data obtained were fitted to different rate equations based on L–H or Eley–Rideal type models. In order to estimate the kinetic constants, the individual rate equations were subjected to a nonlinear regression analysis to estimate the kinetic constants such that the difference between the experimental and the predicted rate has a minimum value. The regression analysis on the experimental data was performed purely on the mathematical basis, and therefore did not account for the thermodynamic significance of the kinetic constants. Several models based on different mechanisms and different rate limiting steps were used for regression analysis (Chaudhari et al., 1983; Andersson et al., 1986). For simple reactions like these, it is possible to formulate different rate equations using L–H approach. The L–H model for catalytic reactions typically involves a sequence of three steps:

1. Adsorption of the reactants.
2. Surface reaction.
3. Desorption of the products.

For each of the individual reactions shown in Fig. 18, these steps occur on palladium sites represented by (s), (s_1) and (s_2) where (s) represents the palladium site for a competitive reaction, and (s_1) and (s_2) represent the palladium sites for non-competitive reaction. The mechanistic schemes for both reactions are shown in Figs. 19 and 20, respectively. Based on these mechanisms, different rate equations are derived considering each step as the rate limiting step for both the reactions. These rate equations are listed in Table 3. The values for the kinetic constants obtained from these rate equations had to satisfy certain conditions, which are derived from the thermodynamic, and optimization considerations. These constraints are

Rule 1: Rate and equilibrium constants should be positive.

Rule 2: $E_a > 0$ (Activation energy should be positive).

Rule 3: R^2 (optimization variable) $> 95\%$.

Rule 4: The confidence intervals of the parameter values should be much less than the values themselves.

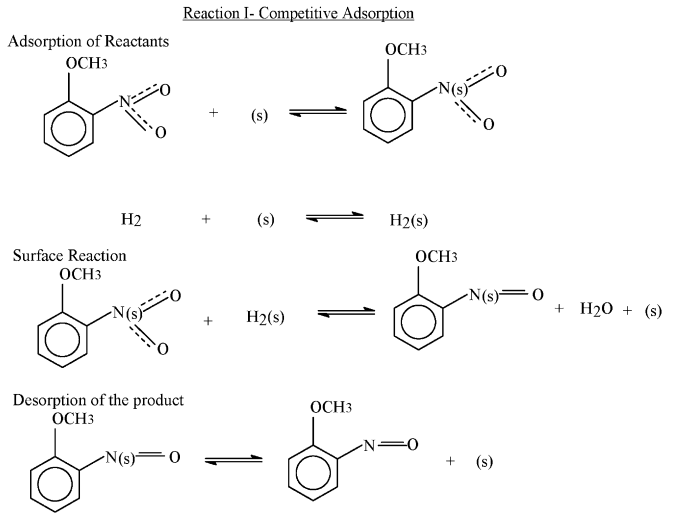

Fig. 19. Mechanistic scheme for reaction 1.

Based on all of the above criteria, the rate equations (from Table 1) that best fitted the experimental data for reactions I and II are the following:

For reaction I (desorption of the product controlling)

$$r_1 = k_I C_{H_2} C_N / (1 + K_N C_N)(1 + K_{H_2 I} C_{H_2}). \quad (5)$$

For reaction II (surface reaction 1 controlling)

$$r_2 = k_{II} K_{H_2 II} C_{H_2} K_I C_I / (1 + K_I C_I)(1 + K_{H_2 II} C_{H_2}), \quad (6)$$

where k_I and k_{II} are the rate constants for reactions I and II, respectively, K_N, $K_{H_2 I}$, K_I and $K_{H_2 II}$ are adsorption equilibrium constants, C_{H_2}, C_N and C_I are concentrations of hydrogen, *o*-nitroanisole and 2-nitrosomethoxybenzene, respectively.

The values of the kinetic constants obtained using the optimization program for these models are given in Table 2. The rates predicted from the rate equations agree with the experimental rates within 10% error. The activation energies and heat of adsorption of the reactants for reactions I and II were determined from the kinetic constants using the Arrhenius equations:

For rate constant

$$k = k_0 e^{-E_a/RT}. \quad (7)$$

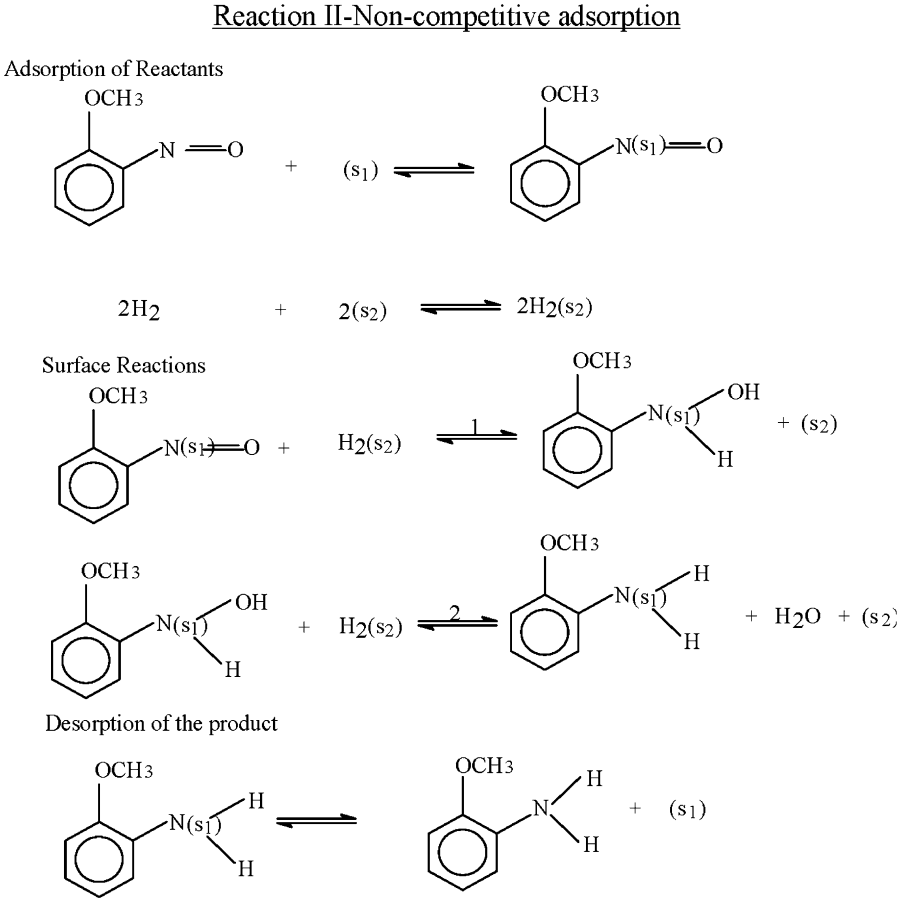

Fig. 20. Mechanistic scheme for reaction 2.

Table 1
Rate equations derived from L–H mechanism

No.	Rate limiting step	Rate equation
Reaction I		
1	Adsorption of *o*-nitroanisole	$r_1 = k_I(C_N)/(1 + (K_{H_2I}C_{H_2})$
2	Adsorption of hydrogen	$r_1 = k_I(C_{H_2})/(1 + (K_N C_N)$
3	Surface reaction	$r_1 = k_I(K_{H_2I}C_{H_2})(K_N C_N)/(1 + (K_N C_N) + (K_{H_2I}C_{H_2}))$
4	Desorption of 2-methoxy nitroso benzene	$r_1 = k_I(C_{H_2}C_N)/((1 + (K_N C_N))(1 + (K_{H_2I}C_{H_2})))$
Reaction II		
1	Adsorption of 2-methoxy nitroso benzene	$r_2 = k_{II}(C_I)$
2	Adsorption of hydrogen	$r_2 = k_{II}(C_{H_2})$
3	Surface reaction 1	$r_2 = k_{II}(K_{H_2II}C_{H_2})(K_I C_I)/((1 + (K_I C_I))(1 + (K_{H_2II}C_{H_2})))$
4	Surface reaction 2	$r_2 = k_{II}K(K_{H_2II}C_{H_2})^2(K_I C_I)/((1 + (K_I C_I) + (K_a K_I K_{H_2II} C_I C_{H_2}))(1 + (K_{H_2II}C_{H_2})))$
5	Desorption of *o*-anisidine	$r_2 = k_{II}(K(K_{H_2II}C_{H_2})^2(K_I C_I))/(1 + (K_I C_I) + (K_a K_I K_{H_2II} C_I C_{H_2}(1 + (K_b K_{H_2II} C_{H_2})))$

Table 2
Kinetic constants and regression coefficients for the reactions

Temp. (°C)	k_I (L^2/g h mol)	K_N(L/mol)	K_{H_2I} (L/mol)	R^2
Reaction I				
30	620.15 ± 4.06	2.00 ± 0.018	0.24 ± 0.006	0.97
40	1556.07 ± 6.67	3.14 ± 0.017	1.38 ± 0.04	0.984
50	3100.00 ± 18.69	3.93 ± 0.03	2.61 ± 0.06	0.965
Temp. (°C)	k_{II} (mol/g h)	K_I (L/mol)	K_{H_2II} (L/mol)	R^2
Reaction II				
30	149.1 ± 0.045	11.09 ± 0.084	2.25 ± 0.01	0.954
40	216.9 ± 1.57	6.78 ± 0.096	4.02 ± 0.04	0.972
50	404.99 ± 3.75	3.29 ± 0.044	4.41 ± 0.06	0.957

For equilibrium constants

$$K = K_0 e^{-\Delta H/RT}, \tag{8}$$

where k is the rate constant for the reaction, k_0 is the pre-exponential factor for the reaction, E_a is the activation energy for the reaction, K is the equilibrium constant for the reactant, K_0 is the pre-exponential factor for the reactant, ΔH is the heat of adsorption for the reactant and T is the temperature in Kelvin. The pre-exponential factors, activation energies and heat of adsorption of reactants calculated using the Arrhenius equations for various kinetics constants are given in Table 3.

In order to further establish the validity of the above rate equations, and associated kinetic parameters of the overall reaction, a comparison was made between the experimental data obtained under integral conditions, and the theoretical predictions from the above rate equations. To derive the integral model based on the rate equations, the following assumptions were made: (1) isothermal conditions prevail in the reactor, (2) there are no mass transfer effects, and (3) change in the volume due to the reaction is negligible.

The rate of change of *o*-nitroanisole, intermediate, hydrogen and *o*-anisidine per unit length of the reactor are given by the following equations:

$$\frac{dF_{nitro}}{dz} = a(-r_1), \tag{9}$$

Table 3
Pre-exponential factors, activation energies and heats of adsorption for the reactions

Pre-exponential factor	
Reaction I	
k_{I0} (L^2/g h mol)	1.27E + 14
K_{N0} (L/mol)	1.08E + 05
K_{H_2I0} (L/mol)	1.26E + 16
Reaction II	
k_{II0} (mol/g h)	1.37E + 09
K_{I0} (L/mol)	3.59E − 08
K_{H_2II0} (L/mol)	1.35E + 05
Activation energy and heats of adsorption	
Reaction I	
E_a (kJ/mol)	65.55
ΔH_N (kJ/mol)	27.36
ΔH_{H_2I} (kJ/mol)	96.52
Reaction II	
E_a (kJ/mol)	40.5
ΔH_I (kJ/mol)	−49.36
ΔH_{H_2II} (kJ/mol)	27.53

$$\frac{dF_{intermediate}}{dz} = a(r_1 - r_2), \tag{10}$$

$$\frac{dF_{hydrogen}}{dz} = a(-r_1 - 2r_2), \tag{11}$$

$$\frac{dF_{anisidine}}{dz} = a(r_2), \tag{12}$$

where F_{nitro}, $F_{intermediate}$, $F_{hydrogen}$, and $F_{anisidine}$ are molar flow rates of *o*-nitroanisole, intermediate, hydrogen, and *o*-anisidine, respectively, at the given instance, a is the amount of catalyst per unit length of the reactor, and r_1 and r_2 are the reaction rates for equations (5) and (6), respectively. Eqs. (9)–(12) were solved using Runge–Kutta method with the following entrance conditions: at $z = 0$, $F_{nitro} = 0.003622566$ mol/h, $F_{hydrogen} = 0.01338491$ mol/h, $F_{intermediate} = 0$, and $F_{anisidine} = 0$ at a liquid flow rate of 0.05 mol/min and gas flow rate of 5 sccm.

Experiments were carried out with these initial conditions at different hydrogen pressures and different amounts of catalysts

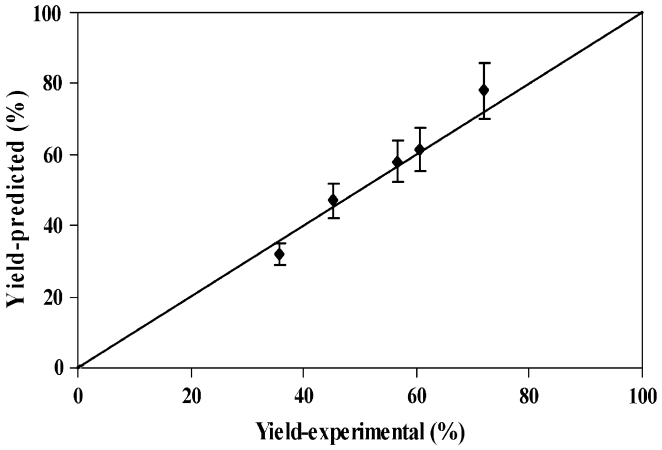

Fig. 21. Experimental and predicted conversion of *o*-nitroanisole for an integral reactor.

but keeping the same residence time. The model predictions and experimental data for the yield of *o*-anisidine under these operating conditions are shown in Fig. 21, and are within 5–10% of each other. This excellent agreement suggests that the rate parameters determined here represent the results obtained under both differential and integral conditions. Under actual operating conditions, mass transfer effects which may be significant need to be incorporated in the analysis.

4. Conclusions

Hydrogenation of *o*-nitroanisole to *o*-anisidine was investigated in a microreactor packed with 2% Pd/zeolite catalyst. The microreactor performance was evaluated by studying the effects of different operating conditions, intraparticle diffusion, gas–liquid and liquid-solid mass transfer, heat transfer, and surface reaction kinetics. The experimental results indicate that the heat and mass transfer resistances were negligible for a wide range of operating conditions and this reaction is kinetically controlled in the microreactor. It was observed through calculations that the gas–liquid mass transfer coefficient in the microreactor is much higher than the estimates obtained from standard correlations in conventional reactors.

The rate of formation of *o*-anisidine was found to be lower than the rate of *o*-nitroanisole disappearance indicating that the intermediate 2-methoxynitrosobenzene was present in significant amount in the reactor at low conversions. Thus, two separate reaction steps were identified: the reduction of *o*-nitroanisole to 2-methoxynitrosobenzene and the further reduction of 2-methoxynitrosobenzene to *o*-anisidine. L–H type rate expressions were found to be suitable for these reaction steps with desorption of 2-methoxynitrosobenzene controlling the first reaction step, and surface reaction controlling the second reaction step. A set of rate equations were obtained based on experimental kinetic data in a differential microreactor. Furthermore, the obtained kinetics were used to predict the integral reactor behavior and found to agree very well.

Although several fast hydrogenation reactions have been conducted in microreactors, there are limited studies on the use of microreactor for obtaining intrinsic kinetics in spite of the excellent mass transfer characteristics it offers. The present study has exploited the advantages of microreactor for obtaining the intrinsic kinetics of the hydrogenation of *o*-nitroanisole reaction for a wide range of operating conditions, thus extending its capability to extremely fast reactions that are controlled by mass transfer in conventional reactors.

Notation

a	amount of catalyst per unit length of the reactor, g/m
a_{gl}	gas–liquid interfacial area, m^2/m^3
a_{ls}	liquid–solid interfacial area, m^2/m^3
b	ratio of diluent to catalyst volume, dimensionless
Bi	Biot's number, dimensionless
C_{H_2}	concentration of hydrogen in the liquid mixture, mol/L
C_N	concentration of nitroanisole in the liquid mixture, mol/L
C_I	concentration of intermediate in the liquid mixture, mol/L
C_s	concentration of the limiting reactant on the surface of the catalyst, mol/L
$C_{H_2,sat}$	saturation concentration of hydrogen at the gas–liquid interface obtained from the hydrogen solubility data, mol/m^3
$C_{H_2,bulk}$	concentration of the hydrogen in the bulk liquid, mol/m^3
$C_{H_2,s}$	concentration of the hydrogen at the solid/liquid interface, mol/m^3
d_p	diameter of the catalyst particle, μm
Da	Damkőhler number for heat transfer, dimensionless
D_e	effective diffusion coefficient of hydrogen in the particle, cm^2/s
D_{H_2}	diffusivity of hydrogen in the liquid obtained from Wilke Chang equation (Perry and Green, 1997), cm^2/s
D_m	hydrogen diffusion coefficient in the liquid reactant, cm^2/s
E_a	activation energy, kJ/mol
$F_{anisidine}$	molar flow rate of *o*-anisidine, mol/h
$F_{hydrogen}$	molar flow rate of hydrogen, mol/h
$F_{intermediate}$	molar flow rate of intermediate, mol/h
F_{nitro}	molar flow rate of *o*-nitroanisole, mol/h
h	heat transfer coefficient for the reactants, $W/m^2\,K$
k_0	pre-exponential factor for reaction, mol/g h
k_I	intrinsic kinetic rate constant for reaction I, $L^2/g\,h\,mol$
k_{II}	intrinsic kinetic rate constant for reaction II, mol/g h
k_{gl}	liquid side mass transfer coefficient, m/s

k_{ls}	liquid/solid mass transfer coefficient, m/s
k_{I0}	pre-exponential factor for the reaction I, $L^2/g\,h\,mol$
k_{II0}	pre-exponential factor for the reaction II, mol/g h
K	equilibrium constant, L/mol
K_a	equilibrium constant, L/mol
k_b	equilibrium constant, L/mol
K_0	pre-exponential factor for reactant, L/mol
K_{H_2I0}	pre-exponential factor for hydrogen in reaction I, L/mol
K_{H_2I}	equilibrium constant for hydrogen in reaction I, L/mol
K_{H_2II0}	pre-exponential factor for hydrogen in reaction II, L/mol
K_{H_2II}	equilibrium constant for hydrogen in reaction II, L/mol
K_I	equilibrium constant for intermediate, L/mol
K_{I0}	pre-exponential factor for intermediate, L/mol
K_N	equilibrium constant for *o*-nitroanisole, L/mol
K_{N0}	pre-exponential factor for nitroanisole, L/mol
L_p	characteristic length of the catalyst particle, cm
r	reaction rate, mol/g cat s
r_{obs}	observed reaction rate, mol/m^3 s
r_1	reaction rate for reaction I, mol/g h
r_2	reaction rate for reaction II, mol/g h
R_{gl}	rate of gas–liquid mass transfer,mol/m^3 s
R_{ls}	rate of liquid-solid mass transfer, mol/m^3 s
R	universal gas constant, J/mol K
R^2	regression coefficient, dimensionless
R_0	radius of the tubular reactor, m
R_{obs}	observed reaction rate, mol/m^3 s
STY	space–time yield, g prod./(g cat h)
T	reaction temperature, K
T_w	reactor wall temperature, K
z	distance from the entrance of the reactor, m

Greek letters

α_1	ratio of observed reaction rate to maximum gas–liquid mass transfer rate, dimensionless
α_2	ratio of observed reaction rate to maximum liquid–solid mass transfer rate, dimensionless
δ	catalyst constriction factor, dimensionless
ΔH	enthalpy of reaction, kJ/mol
ΔH_N	heat of adsorption of nitroanisole, kJ/mol
ΔH_{H_2I}	heat of adsorption of hydrogen for reaction I, kJ/mol
ΔH_{H_2II}	heat of adsorption of hydrogen for reaction II, kJ/mol
ΔH_I	heat of adsorption of intermediate, kJ/mol
ε	void fraction of catalyst bed, dimensionless
η_{eff}	catalyst effectiveness factor, dimensionless
θ	catalyst porosity, dimensionless
λ	effective thermal conductivity of porous catalyst, W/m K
ρ_p	density of catalyst particles, g/m^3
τ	catalyst tortuosity factor, dimensionless
ϕ	Thiele modulus, dimensionless

Acknowledgments

This work is funded by the DOE-ITP under Contract DE-FC36-02GO13156. The authors gratefully acknowledge the support. We would also like to acknowledge our industrial partners from Bristol-Myers Squibb (BMS) especially Dr. Jale Muslehiddinoglu for her technical contributions to the study. We would also like to thank Prof. Suphan Kovenklioglu for his helpful suggestions, and all the members of NJCMCS especially Dr. Dongying Qian and Yuri Voloshin for their help throughout the research work.

References

Ajmera, S.K., Delattre, C., Schmidth, M.A., Jensen, K.F., 2002. Microfabricated differential reactor for heterogeneous gas phase catalyst testing. Journal of Catalysis 209, 401–412.

Andersson, B., Hatziantoniou, V., Schöön, N., 1986. Mass transfer and selectivity in liquid-phase hydrogenation of nitro compounds in a monolithic catalyst reactor with segmented gas–liquid flow. Industrial and Engineering Chemistry Process Design and Development 25, 964–970.

Besser, R.S., Ouyang, X., 2005. Effect of reactor heat transfer limitations on CO preferential oxidation. Journal of Power Sources 141, 39–46.

Besser, R.S., Ouyang, X., Bednarova, L., Ho, P., 2005. Preferential oxidation (PrOx) in a thin-film catalytic microreactor: advantages and limitations. A.I.Ch.E. Journal 51, 1758–1772.

Blaser, H.U., Siegrist, U., Steiner, H., 2001. Fine Chemicals through Heterogeneous Catalysis. Wiley/VCH, Weinheim. p. 389.

Brahme, P.H., Vadgaonkar, H.G., Ozarde, P.S., Parande, M.G., 1982. Solubility of hydrogen in *o*-nitroanisole, *o*-nitroanisole-methanol mixtures and *o*-anisidine. Journal of Chemical and Engineering Data 27, 461–462.

Broekhuis, R.R., Machado, R.M., Nordquist, A.F., 2001. The ejector driven monolith loop reactor—experiments and modelling. Catalysis Today 69 (1–4), 93–97.

Chaudhari, R.V., Parande, M.G., Ramachandran, P.A., Brahme, P.H., 1983. Modelling of a batch slurry reactor for hydrogenation of *o*-nitroanisole to *o*-anisidine. Institute of Chemical Engineers Symposium Series No. 87, pp. 205–213.

Figueras, F., Coq, B., 2001. Hydrogenation and hydrogenolysis of nitro-, nitroso-, azo-, azoxy- and other nitrogen-containing compounds on palladium. Journal of Molecular Catalysis A: Chemical 173, 223–230.

Födisch, R., Kursawe, A., HConicke, D., 2002. Immobilizing heterogeneous catalysts in microchannel reactors. In: Proceedings of the Sixth International Conference on Microreaction Technology, New Orleans, pp. 140–146.

Frikha, N., Schaer, E., Houzelot, J., 2006. Methodology of multiphase reaction kinetics and hydrodynamics identification: application to catalyzed nitrobenzene hydrogenation. Chemical Engineering Journal 124, 19–28.

Hessel, V., Jähnisch, K., Baerns, M., Ehrfeld, W., Haverkamp, V., Löwe, H., Wille, Ch., Guber, A.E., 2000. Direct fluorination of toluene using elemental fluorine in gas/liquid microreactors. Journal of Fluorine Chemistry 105, 117–128.

Hessel, V., Yeong, K.K., Gavriilidis, A., Zapf, R., 2003. Catalyst preparation and deactivation issues for nitrobenzene hydrogenation in a microstructured falling film reactor. Catalysis Today 81, 641–651.

Hessel, V., Yeong, K.K., Gavriilidis, A., Zapf, R., 2004. Experimental studies of nitrobenzene hydrogenation in a microstructured falling film reactor. Chemical Engineering Science 59, 3491–3494.

Iliuta, I., Larachi, F., Grandjean, B.P.A., Wild, G., 1999. Gas–liquid interfacial mass transfer in trickle-bed reactors: state-of-the-art correlations. Chemical Engineering Science 54, 5633–5645.

Irandoust, S., Andersson, B., Bengtsson, E., Silverstrom, M., 1989. Scale up of a monolytic catalyst reactor with two-phase flow. Industrial and Engineering Chemistry Research 28, 1489–1493.

Kreutzer, M.T., Du, P., Heiszwolf, J.J., Kapteijn, F., Moulijn, J.A., 2001. Mass transfer characteristics of three-phase monolith reactors. Chemical Engineering Science 56, 6015–6023.

Kreutzer, M.T., Kapteijn, F., Moulijn, J.A., Heiszwolf, J.J., 2005a. Multiphase monolith reactors: chemical reaction engineering of segmented flow in microchannels. Chemical Engineering Science 60, 5895–5916.

Kreutzer, M.T., Kapteijn, F., Moulijn, J.A., 2005b. Fast-gas–liquid–solid reactions in monoliths: a case study of nitro-aromatic hydrogenation. Catalysis Today 105, 421–428.

Liu, W., Roy, S., Fu, X., 2005. Gas–liquid catalytic hydrogenation reaction in small catalyst channel. A.I.Ch.E. Journal 51, 2285–2297.

Losey, M.W., Schmidt, M.A., Jensen, K.F., 2001. Microfabricated multiphase packed-bed reactors: characterization of mass transfer and reactions. Industrial and Engineering Chemistry Research 40, 2555–2562.

Machado, R.M., Parrillo, D.J., Boehme, R.P., Broekhuis, R.R., 1999. Use of a monolith catalyst for the hydrogenation of dinitrotoluene to toluenediamine. US Patent 6005143.

Mahajani, V.V., Haldar, P., 2004. Catalytic transfer hydrogenation: *o*-nitro anisole to *o*-anisidine, some process development aspects. Chemical Engineering Journal 104, 27–33.

Mears, D.E., 1971a. Diagnostic criteria for heat transport limitations in fixed bed reactors. Journal of Catalysis 20, 127–131.

Mears, D.E., 1971b. Test for transport limitations in experimental catalytic reactors. Industrial and Engineering Chemistry Process Design and Development 10, 541–547.

Mills, P.L., Chaudhari, R.V., 1997. Multiphase catalytic reactor engineering and design for pharmaceuticals and fine chemicals. Catalysis Today 37, 367–404.

Neri, G., Musolino, M.G., Milone, C., Visco, A.M., Di Mario, A., 1995. Mechanism of 2, 4-dinitrotoluene hydrogenation over Pd/C. Journal of Molecular Catalysis A: Chemical 95, 235–241.

Nijhuis, T.A., Dautzenberg, F.M., Moulijn, J.A., 2003. Modelling of monolithic and trickle-bed reactors for the hydrogenation of styrene. Chemical Engineering Science 58, 1113–1124.

Perry, R.H., Green, D.W., 1997. Perry's Chemical Engineerings' Handbook. seventh ed.. McGraw-Hill, USA.

Qian, D., Lawal, A., 2006. Numerical study on gas and liquid slugs for Taylor flow in a T-junction microchannel. Chemical Engineering Science 61, 7609–7625.

Satterfield, C.N., 1970. Mass Transfer in Heterogeneous Catalysis. MIT Press, Cambridge, England. p. 86.

Stoessel, F., 1993. Experimental study of thermal hazards during the hydrogenation of aromatic nitro compounds. Journal of Loss Prevention in the Process Industries 6, 79–85.

Versteeg, G.F., Visser, J.B.M., Van Dierendonck, L.L., Kuipers, J.A.M., 1992. Absorption accompanied with chemical reaction in trickle-bed reactors. Chemical Engineering Science 52, 4057–4067.

Winterbottom, J.M., 1981. In: Pearce, R., Paterson, W.R. (Eds.), Catalysis and Chemical Processes. Leonard Hill, London, p. 318.

Winterbottom, J.M., Natividad, R., Kulkarni, R., Nuithitikul, K., Raymahasay, S., Wood, J., 2004. Analysis of the performance of single capillary and multiple capillary (monolith) reactors for the multiphase Pd-catalyzed hydrogenation of 2-Butyne-1,4-Diol. Chemical Engineering Science 59, 5431–5438.

Yao, H.C., Emmett, P.H., 1961. Kinetics of liquid phase hydrogenation. II. Hydrogenation of aromatic and aliphatic nitrocompounds over a colloidal platinum catalyst. Journal of the American Chemical Society 83, 796–799.